

Spectral segmentation and radiomic features predict carotid stenosis and ipsilateral ischemic burden from DECT angiography

Shadi Ebrahimian 

Fatemeh Homayounieh 

Ramandeep Singh 

Andrew Primak 

Mannudeep K. Kalra 

Javier M. Romero 

PURPOSE

The purpose of this study is to compare spectral segmentation, spectral radiomic, and single-energy radiomic features in the assessment of internal and common carotid artery (ICA/CCA) stenosis and prediction of surgical outcome.

METHODS

Our ethical committee–approved, Health Insurance Portability and Accountability Act (HIPAA)-compliant study included 85 patients (mean age, 73 ± 10 years; male : female, 56 : 29) who underwent contrast-enhanced, dual-source dual-energy CT angiography (DECTA) (Siemens Definition Flash) of the neck for assessing ICA/CCA stenosis. Patients with a prior surgical or interventional treatment of carotid stenosis were excluded. Two radiologists graded the severity of carotid stenosis on DECTA images as mild (<50% luminal narrowing), moderate (50%-69%), and severe (>70%) stenosis. Thin-section, low- and high-kV DICOM images from the arterial phase acquisition were processed with a dual-energy CT prototype (DTA, eXamine, Siemens Healthineers) to generate spectral segmentation and radiomic features over regions of interest along the entire length (volume) and separately at a single-section with maximum stenosis. Multiple logistic regressions and area under the receiver operating characteristic curve (AUC) were used for data analysis.

RESULTS

Among 85 patients, 22 ICA/CCAs had normal luminal dimensions and 148 ICA/CCAs had luminal stenosis (mild stenosis: 51, moderate: 38, severe: 59). For differentiating non-severe and severe ICA/CCA stenosis, radiomic features (volume: AUC = 0.94, 95% CI 0.88-0.96; section: AUC = 0.92, 95% CI 0.86-0.93) were significantly better than spectral segmentation features (volume: AUC = 0.86, 95% CI 0.74-0.87; section: AUC = 0.68, 95% CI 0.66-0.78) ($P < .001$). Spectral radiomic features predicted revascularization procedure (AUC = 0.77) and the presence of ipsilateral intracranial ischemic changes (AUC = 0.76).

CONCLUSION

Spectral segmentation and radiomic features from DECTA can differentiate patients with different luminal ICA/CCA stenosis grades.

Stroke is a substantial cause of mortality and morbidity around the world. According to the National Vital Statistics Reports, stroke was the fifth leading cause of death in the United States, claiming 146 383 lives in 2017 at 44.9 deaths per 100 000 population.¹ The National Health Interview Survey reported 7.8 million adults (3.1%) in the United States had a stroke in 2018.² Based on the degree of internal carotid/common carotid artery (ICA/CCA) stenosis, stroke risk varies. Internal carotid/common carotid artery stenosis and plaques are responsible for 15% of stroke.³

In asymptomatic patients with more than 50% stenosis, annual stroke risk is up to 1%.⁴ The stroke risk increases with the increasing severity of stenosis. The therapeutic approach varies with different degrees of stenosis with lifestyle changes for asymptomatic patients with low-grade stenosis. Symptomatic patients with moderate- or high-grade stenosis benefit from medical therapy, carotid endarterectomy, carotid artery angioplasty, and/or stent placement according to the degree of stenosis.⁵

From the Department of Radiology (S.E., F.H., R.S., M.K.K. ✉ mkalra@mgh.harvard.edu, J.M.R.) and MGH Webster Center for Quality and Safety (S.E., F.H., M.K.K.), Massachusetts General Hospital and Harvard Medical School, Boston, Massachusetts, USA Siemens Healthcare USA Inc. (A.P.), Malvern, Pennsylvania, USA.

Received 6 October 2020; revision requested 2 November 2020; last revision received 26 March 2021; accepted 12 April 2021.

DOI: 10.5152/dir.2022.20842

You may cite this article as: Ebrahimian S, Homayounieh F, Singh R, Primak A, Kalra MK, Romero JM. Spectral segmentation and radiomic features predict carotid stenosis and ipsilateral ischemic burden from DECT angiography. *Diagn Interv Radiol.* 2022;28(3):264-274.

The current methods for estimating ICA/CCA stenosis are subjective and include the North American Symptomatic Carotid Endarterectomy Trial (NASCET), the European Carotid Surgery Trial (ECST), and the Common Carotid (CC) method. The estimated degree of stenosis using these three methods varies due to different measurement methods and the risk of inter- and intra-observer variations.⁶ Thus, an objective and quantitative approach for assessing the presence and degree of ICA/CCA stenosis can help physicians identify high-risk patients and determine the best therapeutic option.

Radiomic features involve the extraction of quantitative features from medical images that radiologists cannot visually assess.⁷ Although most prior studies applied radiomic features to oncologic settings, a few vascular studies have reported on its potential.^{8,9} A previous study reported using these features to predict the severity and outcome in patients with coronary artery stenosis.⁸ Another study applied radiomic features to differentiate symptomatic and asymptomatic patients with intracranial atherosclerotic plaques.⁹ However, there is no study on the role of single or dual-energy CT (DECT) radiomics or spectral segmentation features for predicting the severity of ICA/CCA stenosis and the need for endovascular treatment.

The CT imaging with dual-energy/spectral scan mode enables the extraction and quantification of certain spectral segmentation features such as the amount and concentration of iodine and water distribution within a region of interest (ROI).¹⁰ A few studies have assessed radiomic features of DECT-specific images such as iodine maps, virtual non-contrast (VNC), or virtual monoenergetic imaging (VMI),¹¹⁻¹⁴ Prior studies in other body regions including bone marrow, lymph nodes, colon, and

liver have applied quantitative information from DECT to characterize focal and diffuse abnormalities.^{10,15} In our institution, dual-energy CT angiography (DECTA) is the preferred method of imaging patients with suspected or known ICA/CCA stenosis. Our study aimed to compare spectral segmentation, spectral radiomic, and single-energy radiomic features in the assessment of ICA/CCA stenosis and prediction of surgical outcomes.

Methods

Research ethics and disclosures

This study received institutional review board approval (protocol number: 2016P000767) and was compliant with the Health Insurance Portability and Accountability Act. The need for informed consent was waived due to the retrospective nature of the study and no substantial risks to the research subjects.

Patients

We identified 160 consecutive patients from our proprietary Radiology Information System (RIS) search engine, Render. The study included 85 patients (mean \pm standard deviation of age: 73 \pm 10; sex M/F: 56/29) who met the inclusion and exclusion criteria (Figure 1). The inclusion criteria were DECTA of the neck clinically indicated for evaluation of suspected or known ICA/CCA stenosis on a dual-source, second-generation, 128-slice CT scanner (Siemens Definition Flash, Siemens Healthineers). All patients who undergo CT angiography on this scanner are scanned in dual-energy scan mode. Patients scanned on other scanners and with a history of any ICA/CCA revascularization surgery, metallic or dental implants in the region of ICA/CCA stenosis, ICA/CCA stents, or motion artifacts were excluded from the study (n=75 patients). A physician coauthor (with 1-year post-doctoral radiology research experience) identified the eligible cases from the RIS.

DECTA of neck

All DECTA of the neck were performed with dual-energy scan mode using 80 kV (x-ray tube A) and 140 kV with tin filter (x-ray tube B). The protocol uses combined angular and longitudinal modulation type of automatic exposure control (CareDose 4D, Siemens Healthineers) with a quality

reference mAs of 320 mAs for tube A. With dual-energy scan mode on dual-source CT, the quality reference mAs are set only for tube A, and the system automatically selects the corresponding value for tube B. The scanner estimates the applied mAs for both tubes based on the planning radiograph and the first 180° rotation. All patients received an intravenous bolus of 80-100 mL of 350 mg% non-ionic contrast medium, Iohexol 350 mg% (Omnipaque 350, GE Healthcare Inc.). The contrast was administered at 5 mL/s through the right antecubital vein in all patients, followed by 40 mL of normal saline flush. The scan was triggered with a bolus tracking technique with the ROI in the ascending thoracic aorta.

The remaining scan parameters were pitch of 0.5 : 1, gantry rotation time of 0.5 second, 128 \times 0.6 mm detector configuration, and a scanner-determined table speed. Thin-section images (1 mm thickness at 0.5 mm overlap) were reconstructed for both high- and low-kV datasets using standard soft tissue reconstruction kernel with iterative reconstruction technique at a strength of 3 (Admirer, Siemens Healthineers).

Image review

The thin-section images at both low- and high-tube potentials (80 and 140 Sn kV) were de-identified and exported offline. A radiologist (R.S. with 5-year radiology experience) reviewed the images and radiology reports to classify each of the 170 ICA/CCA into those without luminal narrowing and those with different luminal stenosis grades according to the NASCET method.^{16,17} Luminal stenosis was graded as mild, moderate, and severe based on <50%, 50%-70%, and >70% ICA/CCA luminal narrowing compared to the distal luminal dimension of normal ICA. Cases with narrowing of distal ICA due to severe stenosis were instead graded as severe stenosis (near-occlusion). For each ICA/CCA, the annotations were performed at a single image or section with maximum luminal stenosis and all images spanning the entire length of luminal stenosis. The ROI included both the lumen and vessel wall or plaques if present. The presence of any motion or metal streak artifacts in the region of luminal stenosis was recorded.

Each patient's head CT and/or MRI exams were reviewed to record evidence of cerebrovascular ischemic stroke concordant

Main points

- Spectral radiomic and segmentation features could differentiate between different degrees of ICA/CCA stenosis.
- Spectral radiomic features can predict revascularization and intracranial ischemic changes on CT and MRI.
- Spectral radiomic features can differentiate degrees of ICA/CCA stenosis with higher AUCs than segmentation features.

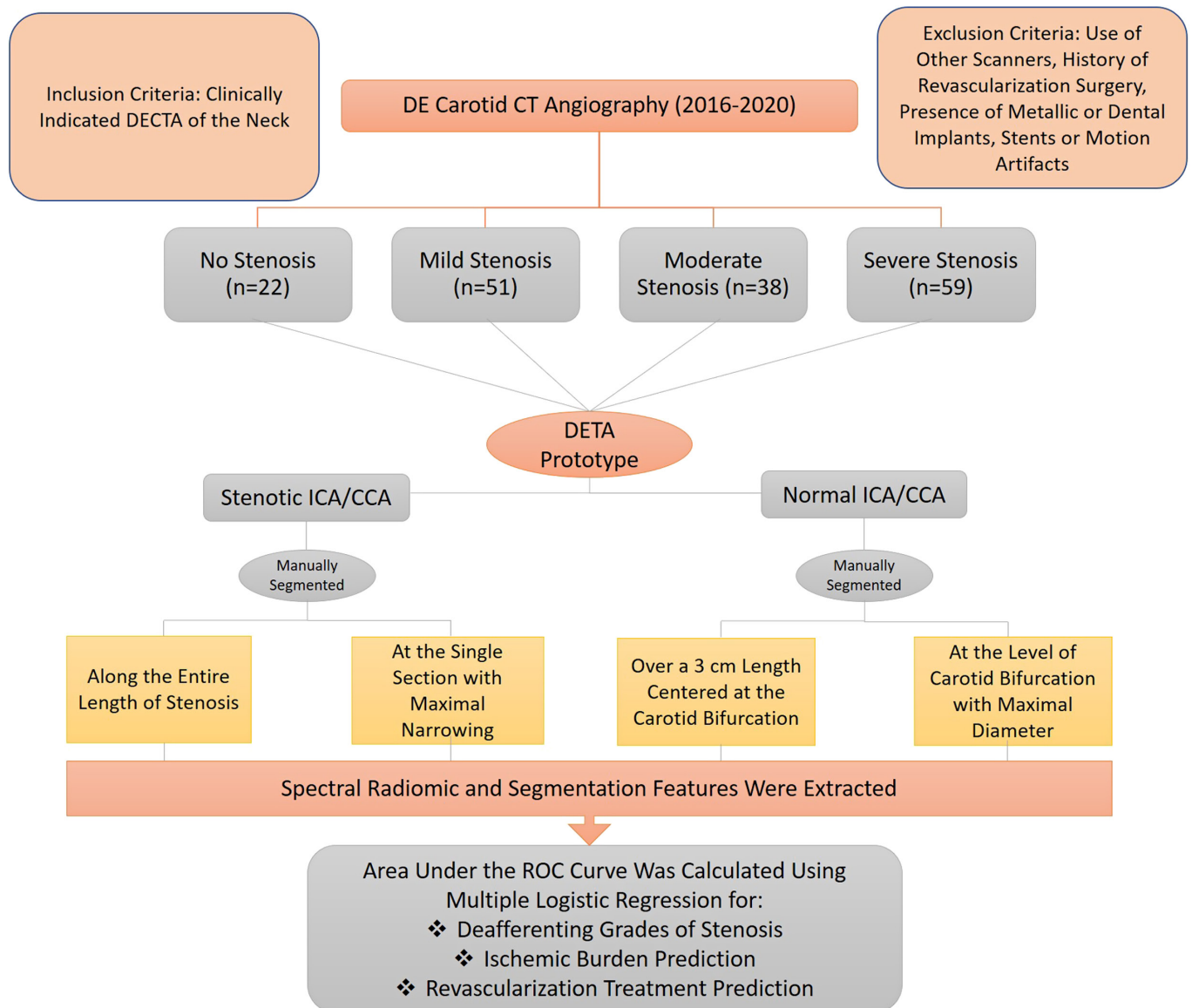


Figure 1. Flow diagram summarizes distribution of ICA/CCA stenosis and inclusion and exclusion criteria as well as evaluation process for obtaining radiomic and segmentation features. ICA/CCA, internal and common carotid artery; DECTA, dual-energy CT angiography; DETA, dual-energy tumor analysis; ROC, receiver operating characteristic.

with the vascular territory of the analyzed vessel. We recorded the history of any revascularization (endarterectomy), including carotid endarterectomy or ICA/CCA stenting following DECTA. The indication for revascularization therapy included severe, symptomatic ICA/CCA stenosis (20/25 patients) in patients with at least 5-year life expectancy and mild or moderate ICA/CCA stenosis and plaques with a history of embolic strokes (5/25 patients). To perform reliability analysis, a second radiologist (M.K.K., 21-year post-radiology residency experience) performed manual segmentation of 50 ICA/CCA in a randomly selected subset of 25 patients.

Post-processing for spectral segmentation

We used a Dual-Energy Tumor Analysis (DETA) prototype (eXamine, Siemens Healthineers) to obtain spectral segmentation and radiomic features over both the section with maximal stenosis and the entire length of stenosis (Figure 2). For ICA/CCA without stenosis, these features were extracted at the carotid bulb section and over a 3 cm length centered at the carotid bifurcation. The prototype enables the use and review of transverse images as well as coronal and sagittal multiplanar images so that segmentation can be performed with the help of any or all of the three planes.

To estimate normalized iodine uptake (the quotient of iodine concentration in the ICA/CCA and the iodine concentration in the aorta), a 1 cm ROI was placed in the aortic arch.

The prototype generates 3 image subtypes, including mixed volume (a linear blend of high- and low-kV images), material decomposition iodine, and water (VNC) images from the thin-section (≤ 1 mm) low- and high-tube potential image series. The use of thin images in our study is in line with previously reported improved performance of radiomic features with a section thickness of 0.5-1 mm.¹⁸ In the next step, the software generates the

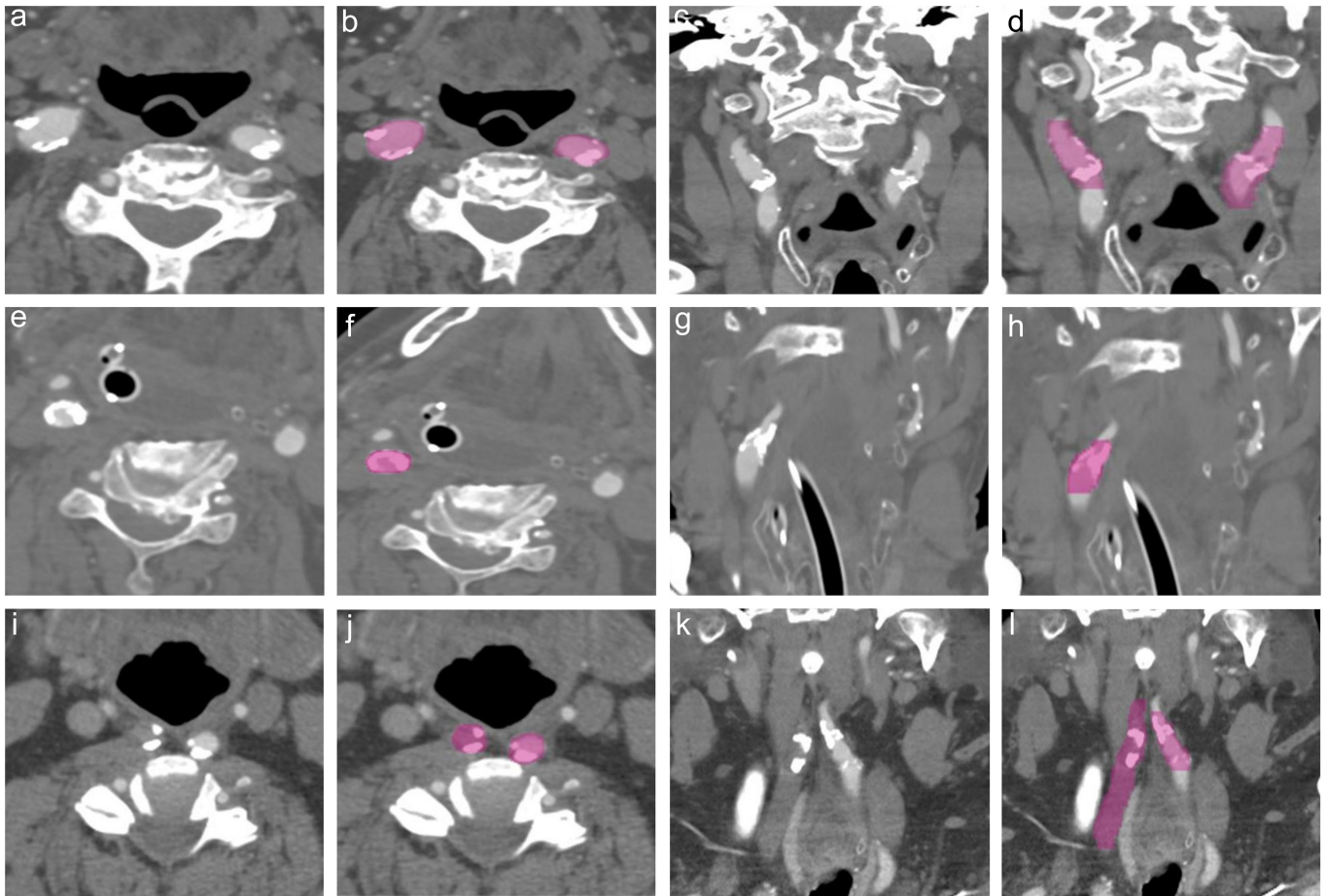


Figure 2. a-l. Transverse (a, b, e, f, i, j) and coronal (c, d, g, h, k, l) multiplanar DECTA images obtained for evaluation of ICA/CCA stenosis in 3 patients. (a-d) Images of a 64-year-old male show unannotated and annotated (in pink) internal carotid arteries with mild luminal stenosis. (e-h) Images of a 78-year-old male depict unannotated and annotated (in pink) internal carotid arteries with moderate stenosis. (i-l) Images of a 77-year-old male demonstrate unannotated and annotated (in pink) ICA/CCA with occlusion.

following spectral features within the ROI—mean mixed CT values (mean HU from mixed volume DECT images), mean iodine CT values (mean HU from material density iodine images), mean VNC CT values (derived by subtracting the mean iodine HU from the mean mixed HU), total iodine uptake (total amount of iodine), total iodine concentration (iodine within per unit volume in mg/mL), vital iodine uptake (iodine uptake within the part of the ROI that excludes the non-enhancing portion), and vital iodine concentration (iodine concentration within the part of the ROI that excludes the non-enhancing portion). These features were estimated for the length of the stenosis and at the level of maximal stenosis.

In addition to spectral segmentation features, radiomic features were derived for the five image series (low kV, high kV, mixed volume, material density iodine, and VNC series). The low- and high-kV radiomic features represent single-energy

radiomics, whereas spectral radiomic features are acquired from mixed-volume and material density images. Both types of radiomics are categorized into shape features, first-order, second-order, and higher-order features.

The shape features describe voxel volume, surface area, sphericity, compactness, maximum diameter, axis length, elongation, and flatness. The first-order statistics features included entropy, minimum, maximum, mean, median, range, interquartile range, 10th percentile, 90th percentile, standard deviation of voxel intensities, skewness (asymmetry), kurtosis (flatness), and uniformity (homogeneity) within the ROI. The second-order statistics were gray-level co-occurrence matrix (GLCM; $n=23$ features), neighboring gray-tone difference matrix (NGTDM; $n=5$), gray-level size zone matrix (GLSZM; $n=16$), gray-level run-length matrix (GLRLM; $n=16$), and gray-level dependence matrix (GLDM, $n=14$). These features indicate heterogeneity within the

ROI by estimating the relationship between neighboring voxels. The higher-order features included square, square root, logarithm, exponential, logarithm, and wavelet transform of the radiomics above.^{19,20}

Our prototype interfaces with the PyRadiomics library for the computation of radiomic features, like 3D Slicer's Radioimcs plugin.^{21,22} This public domain library offers customization of image preprocessing before feature extraction with Laplacian of Gaussian filtering, wavelet filtering, as well as non-linear intensity transforms. The PyRadiomics website standardizes radiomic features for interoperability across datasets. We did not apply any resampling or normalization during calculation of radiomics since we used a single CT scanner (which has absolute gray levels compared to relative signal intensity with MRI) for all included exams, with identical slice thickness, matrix, and pixel size. We used bin-width discretization technique with a bin-width set at 25.

Statistical analysis

For statistical analyses, we imported data on the spectral and radiomic features into another prototype (FRONTIER, Siemens Healthineers). Univariate analysis, multiple, and multivariate logistic regression tests were performed with the area under the receiver operating characteristics curve (AUC) and *P* values for statistical significance as outputs. The cutoff values for best individual features were obtained from Youden J index (MedCalc, Version 19.7.4). In order to determine the best model for multiple logistic regression analysis, t test/ANOVA for each feature is performed to detect the statistical significance. The least significant difference (LSD) post hoc test was performed for significant *P* values in ANOVA analysis. The *P* values are corrected for multiple testing with Benjamini-Hochberg false discovery rate (FDR). Features with a corrected *P* value of <.05 are considered statistically significant and selected for further analysis. For the remaining set of statistically significant features, a minimum redundancy maximum relevance (mRMR) feature selection is applied to eliminate irrelevant and redundant features. To keep the 1-in-10 rule, we limited the mRMR feature selection to four features. With these resulting 4 features, a step-wise forward selection is applied. The best subset is selected using the Akaike information criterion (AIC).²³ A Hosmer-Lemeshow test and Omnibus test were performed to assess the goodness-of-fit for logistic regression and assess if the new model is an improvement over the baseline model. Multinomial logistic regression analysis was performed for the best radiomic features to find the best model for grading stenosis. The logistic

regression analysis was performed using the following formula: x represents the feature values and β values are coefficients, with β_0 as intercept: $f(x) = 1/(1 + e^{-(\beta_0 + \beta_1 x_1 + \beta_2 x_2 + \dots + e_i)})$.

Statistical analyses were performed to compare spectral and single-energy radiomics for the presence and severity of ICA/CCA stenosis. Likewise, the performance of spectral segmentation and radiomics features was compared for the presence of stenosis, different grades of stenosis (severe versus non-severe stenosis), and prediction of invasive revascularization treatment and ischemic changes on brain CT/MRI. Descriptive statistics were given the frequency with percentages and mean \pm standard deviation. Chi-square test was performed to compare categorical variables. T test was performed to compare the means of numerical variables. To compare the AUCs, De-long test was performed. All statistical analyses were performed with python-based statistical tools built into the prototype as well as SPSS statistical program (version 24, IBM).

Results

There were no motion or metal-related artifacts in the regions of ICA/CCA in any patients. Of the 170 ICA/CCA included in our study, 22 (12.94%) ICA/CCA had no luminal stenosis, and the remaining 51 (30.00%) had mild, 38 (22.35%) moderate, or 59 (34.71%) severe stenosis based on the NASCET method^{15,16} (Table 1). Patients with normal and severe stenosis of the carotid lumen were significantly younger than those with mild (*P* = .037) or moderate stenosis (*P* = .013).

Of the 85 patients included in the study, 25 patients (29.41%) underwent a revascularization procedure. Of these 25 patients, 20 had severe (80.00%) ICA/CCA stenosis, 4 had moderate luminal stenosis (16.00%), and 1 patient (4.00%) had mild stenosis (Table 1). Spectral radiomic features (GLDM large-dependence high gray-level emphasis and GLDM low gray-level emphasis) from mixed volume images predicted revascularization procedure with an AUC of 0.77 (95% CI 0.72-0.81) and the presence of ipsilateral intracranial ischemic changes corresponding to the ICA artery territory (30 patients, 35.29%) on head CT and MRI with an AUC of 0.76 (95% CI 0.66-0.85) (Table 1). There was no difference in the AUCs for radiomics from single-section versus the length of luminal stenosis (*P* = .430). Neither spectral segmentation features (AUC = 0.68, 95% CI 0.41-0.86) nor the degree of luminal stenosis (AUC = 0.63, 95% CI 0.45-0.73) were strong predictors of revascularization or the presence of CT/MR finding of stroke in patients with ICA/CCA stenosis.

Both single-energy (AUCs = 0.89-0.91) and spectral (AUCs = 0.92-0.94) had similar AUCs for differentiating severe and non-severe ICA/CCA stenosis from single-section and length-based evaluation of the vessels (*P* = .163). Both single-energy and dual-energy CT radiomic features had identical AUCs (0.99, 95% CI 0.97-1) over the length of ICA/CCA for differentiating ICA/CCA with and without luminal stenosis (*P* = .412). However, single section-based single-energy radiomics had a non-significant lower AUC (0.89, 95% CI 0.83-0.93) for differentiating severe and non-severe stenosis of ICA/CCA as compared to single-section spectral radiomics (AUC = 0.92, 95%

Table 1. Summary of demographics and revascularization in patients with different grades of ICA/CCA stenosis based on the NASCET method

Demographic summary of patients with and without ICA/CCA stenosis					
Patient information	No stenosis	Mild	Moderate	Severe	<i>P</i>
Number of patients*	20 (13.98%)	45 (31.46%)	32 (22.37%)	46 (32.16%)	–
Number of carotid arteries	22 (12.94%)	51 (30.00%)	38 (22.35%)	59 (34.70%)	–
Age (years), mean \pm SD	70 \pm 10	75 \pm 10	76 \pm 8	71 \pm 10	.009
Sex (M/F)	12/10 (54.54%/45.45%)	38/13 (74.51%/25.49%)	20/18 (52.63%/47.37%)	42/17 (71.19%/28.81%)	.084
Enderarterectomy (Y/N)	0/22 (0.00%/100.00%)	1/50 (2.00%/98.00%)	4/34 (10.53%/89.47%)	20/39 (33.90%/66.10%)	<.001
Ischemic changes on CT/MRI (Y/N)	1/21 (4.54%/95.45%)	4/47 (7.84%/92.16%)	10/28 (26.32%/73.68%)	15/44 (25.42%/74.58%)	.016

The frequencies are reported for categorical variables with percentage in parentheses.

ICA/CCA, internal and common carotid artery; NASCET, North American Symptomatic Carotid Enderarterectomy Trial; SD, standard deviation; M/F, male/female; Y/N, yes/no; CT, computed tomography; MRI; magnetic resonance imaging.

*The total number of patients exceed 85 patients as some patients had different grades of stenosis on either side.

CI 0.85-0.96) ($P=.204$). Spectral radiomic features had higher AUCs in differentiating moderate and severe luminal stenosis than single-energy radiomic features over the length of stenosis (AUC = 0.92, 95% CI 0.83-0.95 vs. 0.89, 95% CI 0.83-0.93; $P=.461$) as well as a single section (AUC = 0.86, 95% CI 0.80-0.91 vs. 0.82, 95% CI 0.77-0.85; $P=.359$).

Area under the receiver operating characteristics curves and best predictive spectral segmentation and radiomic features

for differentiating between different ICA/CCA stenosis grades are summarized in Tables 2 and 3. For differentiating non-severe and severe ICA/CCA stenosis, radiomic features (volume: AUC = 0.94, 95% CI 0.88-0.96; section: AUC = 0.92, 95% CI 0.86-0.93) were significantly better than spectral segmentation features (volume: AUC = 0.86, 95% CI 0.74-0.87; section: AUC = 0.68, 95% CI 0.66-0.78) ($P < .001$). Spectral radiomic features from single-section as well as over the length of ICA/CCA (AUC = 0.91,

95% CI 0.82-0.94 and AUC = 0.92, 95% CI 0.87-0.96) had significantly higher AUC compared to corresponding spectral segmentation features (AUC = 0.76, 95% CI 0.62-0.81 and AUC = 0.75, 95% CI 0.64-0.85) for differentiating mild and moderate stenosis and moderate and severe stenosis ($P < .001$) (Figure 3) (Tables 2 and 3). For differentiating mild and normal stenosis, spectral radiomic and segmentation features had similar AUCs ($P = .081$). The best 10 radiomic features for differentiating grades of stenosis on univariate logistic regression analysis are shown in Figure 4.

On the other hand, both spectral segmentation and radiomic features had similar high predictive values for differentiating normal and mild ICA/CCA (Tables 2 and 3). This high predictive value was true at the single-section and over the length of ICA/CCA stenosis.

The highest AUCs for differentiating moderate and severe ICA/CCA stenosis belonged to spectral radiomic features extracted from the length and single-section of ICA/CCA (AUC = 0.92, 95% CI 0.83-0.95 and AUC = 0.86, 95% CI 0.80-0.91) followed by spectral segmentation features over the length and single-section ROIs (AUC = 0.80, 95% CI 0.75-0.82 and AUC = 0.74, 95% CI 0.73-0.77). The cutoff values for the best spectral radiomic and segmentation features are summarized in Tables 2 and 3.

Hosmer-Lemeshow test did not reveal any significant difference in the goodness-of-fit of the model between different grades of stenosis ($P = .342$). Omnibus test revealed a -2 Log likelihood of 65.6, a Nagelkerke R square of 0.66, and P value $< .001$.

The formulae for best spectral radiomics over ICA/CCA length were:

Differentiating normal lumen and mild stenosis: $f(x) = 1/(1+e^{-(-115.6 + 48.5 x_1 - 0.2 x_2 - 118.0 x_3 + 97.5 x_4 + 26.5 x_5)})$ [x_1 : Wavelet-zone entropy (GLSZM); x_2 : Original-10th percentile (first order); x_3 : Wavelet low gray-level zone emphasis (GLSZM); x_4 : Logarithm-lmc2 (GLCM); x_5 : Square root-normalized gray-level non-uniformity (GLSZM)].

Differentiating mild and moderate stenosis: $f(x) = 1/(1+e^{-(-23.9 + 2.0 x_1 + 0.01 x_2 - 17.2 x_3 + 16.9 x_4 - 0.1 x_5 + 0.4 x_6)})$ [x_1 : Square root-joint entropy (GLCM); x_2 : Wavelet large-dependence high gray-level emphasis (GLDM), x_3 : Wavelet-lmc1 (GLCM), x_4 : Square-maximum probability (GLCM), x_5 : Logarithm-size zone non-uniformity (GLSZM); x_6 : Wavelet-kurtosis (first order)].

Table 2. Summary of the best single-energy radiomic and spectral radiomic and segmentation features over the single section with maximum ICA/CCA stenosis as well as AUCs and P values based on multiple logistic regression

Best spectral radiomic and segmentation features for single-section data			
	Best features	AUC (95% CI)	P
Severe vs. moderate stenosis			
Single-energy	Exponential-dependence variance (GLDM) (≤ 44.5) + original-minimum (first order) (≤ 968)	0.82 (0.77-0.85)	.003
Spectral radiomic	Logarithm-dependence variance (GLDM) (≤ 50.9) + original-minimum (first order) (≤ 988) + exponential-dependence variance (GLDM) (≤ 41.3)	0.86 (0.80-0.91)	.013
Spectral segmentation	Maximum iodine histogram index (≤ 1762)	0.74 (0.73-0.77)	$< .001$
Moderate vs. mild stenosis			
Single-energy radiomic	Original-maximum probability (GLCM) (≤ 0.1) + original-Maximum 2D diameter (shape) (> 11.6) + Wavelet-normalized dependence non-uniformity (GLDM) (≤ 0.08)	0.86 (0.80-0.89)	.031
Spectral radiomic	Original-dependence variance (GLDM) (≤ 42.7) + square root large dependence high gray-level emphasis (GLDM) (≤ 10111) + Exponential small-dependence low gray-level emphasis (GLDM) (> 0.003) + Wavelet-lmc1 (GLCM) (≤ 0.9) + exponential-lmc1 (GLCM) (> -0.3)	0.91 (0.82-0.94)	.036
Spectral segmentation	Mean Vnc (> 103.9) + mean mixed (> 313.9)	0.76 (0.62-0.81)	.034
Mild vs. normal lumen			
Single-energy radiomic	Logarithm-lmc2 (GLCM) (> 0.8) + logarithm-skewness (first order) (> -1.1) + exponential-maximum probability (GLCM) (≤ 0.9) + square root-correlation (GLCM) (> 0.8) + logarithm-run entropy (GLRLM) (> 4.1)	0.99 (0.99-1)	$< .001$
Spectral radiomic	Square root-dependence entropy (GLDM) (> 6.5) + logarithm first order (skewness) (> -1.0) + original-lmc1 (GLCM) (> -0.3) + Wavelet-long-run low gray-level emphasis (GLRLM) (≤ 0.07) + square root-maximum probability (GLCM) (≤ 0.3)	0.99 (0.99-1)	$< .001$
Spectral segmentation	Standard deviation (> 77.2) + max extension Z (> 14) + max iodine histogram index (> 1558) + min iodine histogram index (≤ 1017)	0.99 (0.98-1)	.002

Cutoff values are shown in parentheses for each feature.

Table 3. Summary of the best single-energy radiomic and spectral radiomic and segmentation features over the length of ICA/CCA stenosis as well as AUCs and *P* values based on multiple-logistic regression

Best spectral radiomic and segmentation features along the length of ICA/CCA stenosis		
Best features		AUC (95% CI) <i>P</i>
Severe vs. moderate stenosis		
Single-energy	Original-10th percentile (first order) (≤ 1147) + logarithm-dependence variance (GLDM) (≤ 62.9) + Wavelet-minimum (first order) (> -10.2)	0.89 (0.83-0.93) .026
Spectral radiomics	Original-10th percentile (first order) (≤ 1129) + Wavelet-dependence variance (GLDM) (≤ 38.7) + Wavelet-mean (first order) (≤ 0.1)	0.92 (0.83-0.95) .029
Spectral segmentation	Total iodine concentration (≤ 9.2) + mean mixed (≤ 314.0)	0.80 (0.75-0.82) .018
Moderate vs. mild stenosis		
Single-energy	Square root- <i>l</i> dn (GLCM) (≤ 0.9) + Wavelet- <i>l</i> mc1 (GLCM) (≤ -0.007) + Wavelet-median (first order) (≤ -0.01)	0.87 (0.77-0.90) .032
Spectral radiomic	Square root-joint entropy (GLCM) (> 6.8) + Wavelet-large dependence high gray-level emphasis (GLDM) (≤ 65430) + Wavelet- <i>l</i> mc1 (GLCM) (> -0.2) + square-maximum probability (GLCM) (≤ 0.2) + logarithm-size zone non-uniformity (GLSZM) (> 48.8) + Wavelet-kurtosis (first order) (≤ 9.3)	0.92 (0.87-0.96) .020
Spectral segmentation	Mean Vnc (> 103.9)	0.75 (0.64-0.85) $< .001$
Mild vs. normal lumen		
Single-energy	Original-normalized gray-level non-uniformity (GLSZM) (≤ 0.08) + Wavelet-uniformity (first order) (≤ 0.5) + original-10th percentile (first order) (≤ 1215) + Wavelet-low gray-level emphasis (GLDM) (≤ 0.6) + logarithm-normalized gray-level non-uniformity (GLSZM) (≤ 0.2) + exponential- <i>l</i> mc1 (GLCM) (≤ -0.2)	0.98 (0.97-0.99) .003
Spectral radiomic	Wavelet-zone entropy (GLSZM) (> 6.6) + original-10th percentile (first order) (≤ 1133) + Wavelet-low gray-level zone emphasis (GLSZM) (≤ 0.4) + logarithm- <i>l</i> mc2 (GLCM) (> 0.8) + square root-normalized gray-level non-uniformity (GLSZM) (≤ 0.1)	0.99 (0.98-0.99) .015
Spectral segmentation	Standard deviation (> 77.2) + max extension Z (> 14) + max iodine histogram index (> 534) + min iodine histogram index (≤ 1017)	0.99 (0.97-0.99) .002

Cutoff values are shown in parentheses for each feature.

Differentiating moderate and severe stenosis: $f(x) = 1/(1 + e^{-(46.6 - 0.1 x_1 - 0.3 x_2 - 8.3 x_3)})$ [x_1 : Original-10th percentile (first order); x_2 : Wavelet-dependence variance (GLDM); x_3 : Wavelet-mean (first order)].

Using multivariate logistic regression model, spectral radiomic features over the length could differentiate between

different grades of stenosis with an AUC of 0.94 (95% CI 0.88-0.96) for the combination of square root large-dependence high gray-level emphasis (GLDM) (OR=5.9, 95% CI 2.0-16.5, $P=.001$), original-10 percentile (first order) (OR=5.9, 95% CI 2.8-12.9, $P < .001$), Wavelet-dependence variance (GLDM) (OR=1.8, 95% CI 0.9-3.3, $P=.053$),

and Wavelet-inverse variance (GLCM) (OR=2.8, 95% CI 1.4-5.5, $P=.002$). Spectral segmentation features could differentiate between four grades of stenosis with an AUC of 0.86 (0.74-0.91) for the combination of vital iodine concentration (OR=55.3, 95% CI 14.6-209.9, $P < .001$) and mean mixed (OR=18.1, 95% CI 5.9-54.5, $P < .001$).

Multinomial regression analysis revealed an overall sensitivity of 66.9% and 93.2% for differentiating mild, moderate, and severe stenosis from the best segmentation and radiomic features with a $P=.850$ for the model goodness-of-fit (Table 4).

Both radiologists obtained high AUCs for spectral radiomics (AUC, radiologist 1=0.95-0.99 vs. AUC, radiologist 2=0.98-1.00) and spectral segmentation features (AUC, radiologist 1=0.78-0.89 vs. AUC, radiologist 2=0.89-0.95) for differentiating different grades of ICA/CCA stenosis.

Discussion

Spectral radiomic features extracted from the length of stenosis were the best differentiator of normal and stenotic ICA/CCA, severe and non-severe stenosis, and moderate and severe stenosis of ICA/CCA (per NASCET method) compared to spectral segmentation and single-energy radiomic features. Among these, the first- and higher-order spectral radiomic features were the best predictors of abnormal ICA/CCAs, as well as different grades of luminal stenosis. Although not as strong, the spectral segmentation and single-energy radiomic features were good differentiators of severe and non-severe ICA/CCA stenosis and normal and stenotic ICA/CCA. There are no published studies on the use of spectral radiomic or segmentation features for assessing ICA/CCA stenosis. Prior studies have reported on radiomics in ultrasound and single-energy CT of carotid arteries.²⁴⁻²⁶ Acharya et al. reported an 88% accuracy and specificity of about 87% for classifying symptomatic and asymptomatic carotid plaques with machine learning-based radiomic features from single-energy CT.²⁴ Spectral radiomic features in our study could also predict both revascularization and intracranial ischemic changes on CT and MRI. The ability to detect and classify the severity of ICA/CCA stenosis in our study with both single- and dual-energy features is in line with the prior study from Acharya et al., who reported the ability to estimate luminal stenosis from radiomics.²⁴

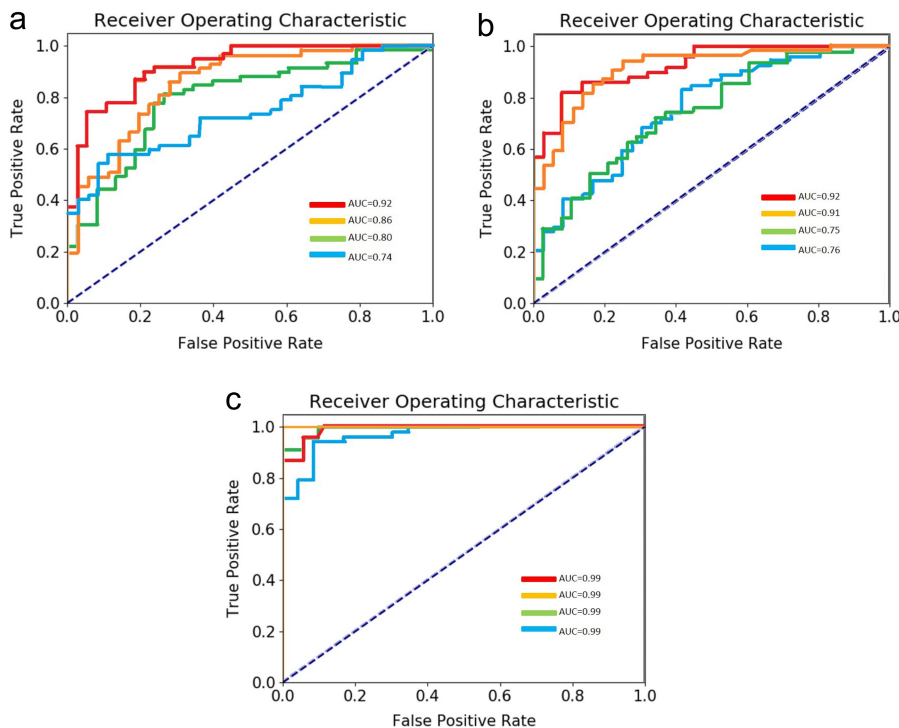


Figure 3. a-c. Moderate vs. severe stenosis (a): AUC=0.92 belongs to spectral radiomics (the length of ICA/CCA stenosis); AUC=0.86 belongs to spectral radiomics (for single-section data); AUC=0.80 belongs to spectral segmentation (the length of ICA/CCA stenosis); and AUC=0.74 belongs to spectral segmentation (for single-section data). Mild vs. moderate stenosis (b): AUC=0.92 belongs to spectral radiomics (the length of ICA/CCA stenosis); AUC=0.91 belongs to spectral radiomics (for single section data); AUC=0.75 belongs to spectral segmentation (the length of ICA/CCA stenosis); and AUC=0.76 belongs to spectral segmentation (for single-section data). Mild stenosis vs. normal lumen (c): AUC=0.99 belongs to spectral radiomics (the length of ICA/CCA stenosis); AUC=0.99 belongs to spectral radiomics (for single-section data); AUC=0.99 belongs to spectral segmentation (the length of ICA/CCA stenosis); and AUC=0.99 belongs to spectral segmentation (for single-section data).

The presence of material decomposition iodine and water images from DECT provides additional information compared to the single-energy CT images. However, only a few studies have assessed the performance of spectral radiomic features. In a study of metastatic lymph nodes in patients with gastric adenocarcinoma, spectral radiomic features predicted the presence of lymph nodal metastases in both arterial (AUC=0.71) and venous (AUC=0.76) phases.¹⁶ Zhou et al. reported improved diagnostic performance for differentiating metastatic and non-metastatic cervical lymph nodes in patients with papillary thyroid carcinoma with radiomic features from DECT-derived iodine maps than with the conventional CT imaging features.¹³

Beyond carotid arteries, Inoue and colleagues reported using texture features to differentiate stable and vulnerable coronary plaques.²⁷ Most studies on ICA/CCA atherosclerosis focus on evaluating and quantifying atherosclerotic plaques

and calcium burden.^{28,29} The amount of ICA/CCA calcification, stenosis, and the unstable fibrous cap is related to a higher stroke rate.²⁹ Unlike previous studies, which were limited to the evaluation of carotid plaques and calcium burden, we performed a combined assessment of both the plaques and lumen of the ICA/CCA.²⁸⁻³⁰ Since our regions of interest included both the plaque and lumen of ICA/CCA, the performance of radiomic and spectral segmentation features was likely a result of combining information related to both the plaques and the luminal dimension. With a greater degree of luminal stenosis, the plaque volume and its CT numbers have a greater contribution to radiomics and spectral segmentation features than a smaller contribution from the stenosed lumen. Conversely, in patients with no or mild luminal stenosis, luminal contrast contributes to the major share of more homogeneous CT numbers and statistics than smaller and possibly more homogeneous atherosclerotic plaques. Thus, the CT

numbers from plaque's calcified and non-calcified components and luminal contrast vary based on the size and composition of plaque and degree of luminal stenosis (less iodine-related HU in the presence of severe stenosis). Due to these changes in distribution (with larger plaques) and intensity (due to differences in grades of stenosis) of CT numbers and iodine, we obtained high AUCs for radiomic and segmentation features. Also, since DECT can better assess quantitative changes in iodine uptake compared to single-energy CT, it is not surprising that the former outperformed the latter.

The major implication of our study is the ability to predict ipsilateral cerebrovascular stroke, revascularization surgery, and degree of luminal ICA/CCA stenosis with a combined evaluation of vessel wall and the lumen of ICA/CCA with radiomics and spectral segmentation features. The reason radiomics outperformed the degree of luminal stenosis for outcome prediction (revascularization and intracranial ischemic changes) was likely related to the combined evaluation of both the plaques and the lumen. Presently, neither radiomic nor spectral segmentation features are approved for clinical use due to a lack of defined technical requirement and accuracy data related to their use. With increasing scientific evidence, these techniques can become automated and integrated with clinical workflow. For example, as opposed to manual identification and segmentation of ICA/CCA, integration of machine learning-based automatic segmentation of carotid arteries can help bring radiomic and spectral segmentation features closer to an efficient clinical use.^{31,32} Such integration will help save time and make the segmentation process less prone to subjective variations associated with manual segmentation. As in our study, several prior studies have reported using machine learning-based prototypes and methods to simplify and automate complex analyses of hundreds of quantitative features generated from radiomic and segmentation features.^{31,32} Such automation can help identify and reduce specific radiomic and segmentation features to the most important ones. Future studies with larger sample size can define cutoff values for spectral segmentation and radiomic features to distinguish patients with different grades of stenosis and help predict the need for invasive treatment.



Figure 4. a-c. Moderate versus severe stenosis (a), mild versus moderate stenosis (b), and mild stenosis versus normal lumen (c). The 10 best features with highest area under the curves on univariate logistic regression analysis for radiomic features from the length.

Table 4. Confusion matrix, sensitivity, specificity, and accuracy of best radiomic features from the length for differentiating mild, moderate, and severe stenosis using multinomial logistic regression analysis

Observed		Predicted			Sensitivity	Specificity	Accuracy
		Mild	Moderate	Severe			
Radiomic features	Mild	47	4	0	92.2%	94.8%	93.9%
	Moderate	4	33	1	86.6%	96.4%	93.9%
	Severe	1	0	58	98.3%	98.9%	98.6%
Segmentation features	Mild	36	9	6	70.6%	80.4%	77%
	Moderate	9	16	13	42.1%	90%	52.7%
	Severe	10	2	47	79.7%	78.6%	79%

There are a few limitations to our study. Our sample size was limited in terms of the number of overall patients and those in each subgroup of luminal stenosis. This was related to the fact that the assessed proprietary prototype can only process data from dual-source DECT examinations. A substantial number of our patients are scanned with single-energy or non-dual-source DECT techniques. Therefore, our study results may not be generalizable to single- or dual-energy examinations performed on other vendor scanners. A limitation of our study pertains to the lack of reproducibility evaluation since the number of cases in different subgroups (normal versus stenotic ICA/CCA) was insufficient for splitting data into training and test groups to create a machine learning-based model.³³ Likewise, our results may not be generalizable to other sites with different scan acquisition and reconstruction parameters, which can affect the estimation of radiomic features. Another limitation of our study pertains to the exclusion of patients with artifacts (streaks and motion). Although our results may not be reproducible in settings of these artifacts, such artifacts negatively affect the subjective interpretation of ICA/CCA as well. Finally, we performed subjective and manual segmentation of ICA/CCA, which may have introduced bias. Interestingly, a prior study on radiomics of coronary atherosclerotic plaque reported lower reproducibility of plaque segmentation with expert radiologists as compared to non-expert readers.^{34,35} These studies underscore the need for accurate and automatic segmentation of blood vessels. Currently, the prototype cannot automatically identify or segment ICA/CCA.

In conclusion, spectral radiomic and segmentation features are highly predictive of the presence and severity of ICA/CCA stenosis from DECTA when regions of interest include both the vessel wall and the lumen.

Only the spectral radiomic features could predict revascularization surgery and the presence of intracranial ischemic changes.

Conflict of interest disclosure

A.P. is an employee of Siemens Healthineers. For unrelated work, M.K.K. has received a research grant from Siemens Healthineers and compensation for consultation with Globus Medical. Other co-authors have no pertinent financial disclosures.

References

- Kochanek KD, Murphy SL, Xu J, Arias E. Deaths: final data for 2017. *Natl Vital Stat Rep.* 2019;68(9):1-77.
- Available at: <https://www.cdc.gov/nchs/fastats/stroke.htm>.
- Petty GW, Brown Jr RD, Whisnant JP, Sicks JD, O'Fallon WM, Wiebers DO. Ischemic stroke subtypes: a population-based study of functional outcome, survival, and recurrence. *Stroke.* 2000;31(5):1062-1068. [CrossRef]
- Nadareishvili ZG, Rothwell PM, Beletsky V, Pagniello A, Norris JW. Long-term risk of stroke and other vascular events in patients with asymptomatic carotid artery stenosis. *Arch Neurol.* 2002;59(7):1162-1166. [CrossRef]
- Gaba K, Ringleb PA, Halliday A. Asymptomatic carotid stenosis: intervention or best medical therapy? *Curr Neurol Neurosci Rep.* 2018; 18(11):80. [CrossRef]
- Kılıçkap G, Ergun E, Başbay E, Koşar P, Kosar U. Carotid stenosis evaluation by 64-slice CTA: comparison of NASCET, ECST and CC grading methods. *Int J Cardiovasc Imaging.* 2012 ;28(5):1257-1266. [CrossRef]
- Gillies RJ, Kinahan PE, Hricak H. H. Radiomics: images are more than pictures, they are data. *Radiology.* 2016;278(2):563-577. [CrossRef]
- Denzinger F, Wels M, Ravikumar N, et al., eds. Coronary artery plaque characterization from CCTA scans using deep learning and radiomics. International Conference on Medical Image Computing and Computer-Assisted Intervention. Berlin: Springer; 2019.
- Shi Z, Zhu C, Degnan AJ, et al. Identification of high-risk plaque features in intracranial atherosclerosis: initial experience using a radiomic approach. *Eur Radiol.* 2018;28(9):3912-3921. [CrossRef]

- Homayounieh F, Singh R, Nitiwarangkul C, et al. Semiautomatic segmentation and Radiomics for dual-energy CT: a pilot study to differentiate benign and malignant hepatic lesions. *AJR Am J Roentgenol.* 2020;215(2):398-405. [CrossRef]
- Zhou Y, Su GY, Hu H, et al. Radiomics analysis of dual-energy CT-derived iodine maps for diagnosing metastatic cervical lymph nodes in patients with papillary thyroid cancer. *Eur Radiol.* 2020;30(11):6251-6262. [CrossRef]
- Wu J, Zhang Q, Zhao Y, et al. Radiomics analysis of iodine-based material decomposition images with dual energy CT imaging for pre-operatively predicting microsatellite instability status in colorectal cancer. *Front Oncol.* 2019;9:1250. [CrossRef]
- Reinert CP, Krieg EM, Bösmüller H, Horger M. Mid-term response assessment in multiple myeloma using a texture analysis approach on dual energy-CT-derived bone marrow images—A proof of principle study. *Eur J Radiol.* 2020;131:109214. [CrossRef]
- Li J, Dong D, Fang M, et al. Dual-energy CT-based deep learning radiomics can improve lymph node metastasis risk prediction for gastric cancer. *Eur Radiol.* 2020;30(4):2324-2333. [CrossRef]
- Yu Y, Guo L, Hu C, Chen K. Spectral CT imaging in the differential diagnosis of necrotic hepatocellular carcinoma and hepatic abscess. *Clin Radiol.* 2014;69(12):e517-e524. [CrossRef]
- NASCET. Beneficial effect of carotid endarterectomy in symptomatic patients with high-grade carotid stenosis. *N Engl J Med.* 1991;325(7):445-453. [CrossRef]
- Bartlett ES, Walters TD, Symons SP, Fox AJ. Quantification of carotid stenosis on CT angiography. *AJNR Am J Neuroradiol.* 2006;27(1): 13-19.
- Hoye J, Solomon JB, Sauer TJ, Samei E. Quantification of minimum detectable difference in Radiomics features Across lesions and CT imaging conditions. *Acad Radiol.* 2021;28(11): 1570-1581. [CrossRef]
- Rizzo S, Botta F, Raimondi S, et al. Radiomics: the facts and the challenges of image analysis. *Eur Rad Exp.* 2018;2(1):36. [CrossRef]
- Doda Khera RD, Homayounieh F, Lades F, et al. Can dual-energy computed tomography quantitative analysis and radiomics differentiate normal liver from hepatic steatosis and cirrhosis? *J Comput Assist Tomogr.* 2020;44(2):223-229. [CrossRef]

21. Available at: <https://pyradiomics.readthedocs.io/en/latest/features.html> Accessed October 28, 2020.
22. van Griethuysen JJM, Fedorov A, Parmar C, et al. Computational radiomics system to decode the radiographic phenotype. *Cancer Res.* 2017;77(21):e104-e107. [\[CrossRef\]](#)
23. Wels MG, Lades F, Muehlberg A, Suehling M. General purpose radiomics for multi-modal clinical research. In: *Medical imaging 2019: Computer-aided diagnosis* (Vol. 10950, p. 1095046). International Society for Optics and Photonics; 2019.
24. Acharya UR, Sree SV, Mookiah MR, et al. Computed tomography carotid wall plaque characterization using a combination of discrete wavelet transform and texture features: a pilot study. *Proc Inst Mech Eng H.* 2013;227(6):643-654. [\[CrossRef\]](#)
25. Loizou CP, Pattichis CS, Pantziaris M, Kyriacou E, Nicolaides A. Texture feature variability in ultrasound video of the atherosclerotic carotid plaque. *IEEE J Transl Eng Health Med.* 2017;5:1800509. [\[CrossRef\]](#)
26. Awad J, Krasinski A, Parraga G, Fenster A. Texture analysis of carotid artery atherosclerosis from three-dimensional ultrasound images. *Med Phys.* 2010;37(4):1382-1391. [\[CrossRef\]](#)
27. Inoue F, Sato Y, Matsumoto N, Tani S, Uchiyama T. Evaluation of plaque texture by means of multislice computed tomography in patients with acute coronary syndrome and stable angina. *Circ J.* 2004;68(9):840-844. [\[CrossRef\]](#)
28. Zhou J, Chen H, Yang T, Xing C, Jia F. Comparison of predictive ability of computed tomography and magnetic resonance imaging in patients with carotid atherosclerosis complicated with stroke. *Iran J Public Health.* 2019;48(6):1052-1058.
29. Sillesen H, Muntendam P, Adourian A, et al. Carotid plaque burden as a measure of subclinical atherosclerosis: comparison with other tests for subclinical arterial disease in the High Risk Plaque Biomechanics study. *JACC Cardiovasc Imaging.* 2012;5(7):681-689. [\[CrossRef\]](#)
30. Mughal MM, Khan MK, DeMarco JK, Majid A, Shamoun F, Abela GS. Symptomatic and asymptomatic carotid artery plaque. *Expert Rev Cardiovasc Ther.* 2011;9(10):1315-1330. [\[CrossRef\]](#)
31. Hemmati HR, Alizadeh M, Kamali-Asl A, Shirani S. Semi-automated carotid lumen segmentation in computed tomography angiography images. *J Biomed Res.* 2017;31(6):548. [\[CrossRef\]](#)
32. Cuisenaire O, eds. *Fully Automated Segmentation of Carotid and Vertebral Arteries from CTA2009.*
33. Koçak B, Durmaz EŞ, Ateş E, Kılıçkesmez Ö. Radiomics with artificial intelligence: a practical guide for beginners. *Diagn Interv Radiol.* 2019;25(6):485-495. [\[CrossRef\]](#)
34. Kolossváry M, Jávorszky N, Karády J, et al. Effect of vessel wall segmentation on volumetric and radiomic parameters of coronary plaques with adverse characteristics. *J Cardiovasc Comput Tomogr.* 2021;15(2):137-145. [\[CrossRef\]](#)
35. Moss AJ, Williams MC. Can we measure vulnerable plaques on coronary CT angiography with both precision and accuracy? *J Cardiovasc Comput Tomogr.* 2021;15(2):146-147. [\[CrossRef\]](#)